

Strong crystal size effect on deformation twinning

Qian Yu¹, Zhi-Wei Shan^{1,2}, Ju Li³, Xiaoxu Huang⁴, Lin Xiao¹, Jun Sun¹ & Evan Ma^{1,5}

Deformation twinning^{1–6} in crystals is a highly coherent inelastic shearing process that controls the mechanical behaviour of many materials, but its origin and spatio-temporal features are shrouded in mystery. Using micro-compression and *in situ* nano-compression experiments, here we find that the stress required for deformation twinning increases drastically with decreasing sample size of a titanium alloy single crystal^{7,8}, until the sample size is reduced to one micrometre, below which the deformation twinning is entirely replaced by less correlated, ordinary dislocation plasticity. Accompanying the transition in deformation mechanism, the maximum flow stress of the submicrometre-sized pillars was observed to saturate at a value close to titanium's ideal strength^{9,10}. We develop a 'stimulated slip' model to explain the strong size dependence of deformation twinning. The sample size in transition is relatively large and easily accessible in experiments, making our understanding of size dependence^{11–17} relevant for applications.

Explosive growth in the use of small-volume materials such as submicrometre-scale single crystals is driving the exploration of sample-size-dependent mechanical behaviour^{15–17}. At room temperature, the two major mechanisms responsible for the plasticity of materials are ordinary dislocation plasticity (ODP) and deformation twinning. For polycrystalline materials, it has been well-established that regardless of the major deformation mechanism, the apparent strength and the grain size (d_g) follows a Hall–Petch-type behaviour: $\sigma = \sigma_0 + kd_g^{-\alpha}$, where σ is the flow strength, σ_0 and k are size-independent constants and α is an exponent typically between 0.5 and 1. The difference is that the Hall–Petch slope for deformation-twinning-mediated plasticity (k_{DT}) is much larger (up to ten times) than that for ODP (k_{ODP})^{18–20}. In recent years, size effects on the plasticity of surface-confined single crystals have drawn considerable attention^{15–17}. It has been demonstrated that the sample dimension d strongly influences the ODP-mediated deformation and hence the apparent strength^{15–17}, which also follows a power-law behaviour. However, it is yet unknown if deformation-twinning-mediated plasticity would be strongly sample-size-dependent. If so, and if $k_{DT} \gg k_{ODP}$, the power-law scaling for deformation-twinning-mediated plasticity must break down at a much larger sample size than that for ODP-mediated plasticity, because the ideal strength of the crystal⁹ imposes an upper bound on the flow stress—see Supplementary Fig. 1.

We chose a single-crystal Ti alloy as our model system. Deformation twinning is known to play a key part in the deformation of hexagonal-close-packed metals^{7,8} owing to the limited number of dislocation slip systems. For compression of bulk Ti and α -Ti alloys along the c -axis^{8,21–24}, deformation twinning is the geometrically favoured deformation mode and the reported^{8,21–24} twinning systems are $\{11\bar{2}2\}\langle\bar{1}\bar{1}23\rangle$, $\{1124\}\langle\bar{2}243\rangle$ and $\{10\bar{1}1\}\langle\bar{1}012\rangle$. In conventional samples, the twin lamellae in Ti and its alloys have thicknesses ranging from 0.1 to 10 μm and lengths of the order of several

micrometres^{7,8,21–24}. It is then interesting to see what will happen when the sample dimensions are reduced to the same scale or even smaller.

We used a bulk square Ti–5 at.% Al single crystal as the starting material, from which all the samples in this study were cut. The experimental details are described in the Methods and in the Supplementary Information. Supplementary Fig. 2 shows the behaviour of the bulk single crystal under [0001] compression. Profuse deformation twinning is seen, in agreement with the literature²⁴. In micro-compression tests of pillars with $d \geq 1.0 \mu\text{m}$, almost all the deformed samples showed obvious shearing traces on the surfaces. Examples are shown in Fig. 1a and b. A trace analysis of the $d = 1.0 \mu\text{m}$ micro-pillar showed that the shearing occurred on the $\{11\bar{2}2\}$ plane, which is a common twinning plane in hexagonal-close-packed Ti and its alloys. Electron backscatter diffraction (EBSD) analysis of these deformed pillars provides evidence that deformation twinning indeed occurred during compression. Figure 1c and d compare the pole figures of the $d = 8.0 \mu\text{m}$ pillar, before and after the deformation. We observed nearly perfect $\{0001\}$ reflection in the micro-pillar before loading, but after deformation several new orientations that are far from the initial orientation appeared. We identify these new orientations as due to deformation twinning on two types of twinning systems, $\{11\bar{2}2\}\langle\bar{1}\bar{1}23\rangle$, and $\{10\bar{1}1\}\langle\bar{1}012\rangle$, as indicated in Fig. 1d. Similar EBSD results were obtained for the $d = 1.0 \mu\text{m}$ sample as well. Rapid deformation twin growth is also corroborated by the obvious strain bursts in the stress–strain curves; see Fig. 2a. Transmission electron microscopy (TEM) micrographs of the deformed $d = 8 \mu\text{m}$ pillar, taken from its vertical cross-section cut using focused ion beam (FIB) micromachining (Supplementary Fig. 3), are shown in Supplementary Figs 4 and 5: deformation twins are observed inside tangles of curved dislocations. The twins with small sizes—that is, twin embryos—exhibit convex lens shapes (Supplementary Fig. 5), in contrast to the straight profile of grown twin bands (Supplementary Fig. 2).

We noticed remarkable changes in deformation behaviour for $d = 0.7 \mu\text{m}$ and $0.4 \mu\text{m}$. As shown in Fig. 3a and b, in these submicrometre pillars plastic deformation is concentrated on the top part of the pillar, resulting in a 'mushroom' shape. The load-displacement curve of this sample is given in Fig. 2b. In Fig. 2b we observe continuous plastic flow without any major strain burst. This difference from Fig. 2a suggests a dramatic change in the deformation mode as compared with the larger, micrometre-sized pillars.

We also conducted compression tests *in situ* inside a TEM for a 0.25- μm -diameter cylindrical pillar, to reveal the entire dynamic deformation process in these submicrometre pillars (see movie in the Supplementary Information). The still images comparing the structure before and after testing are displayed in Fig. 3c and d. The corresponding load-displacement curve is in Fig. 2c. Here again, we observe the development of mushroom-like sample morphology

¹Center for Advancing Materials Performance from the Nanoscale (CAMP-Nano), State Key Laboratory for Mechanical Behavior of Materials, Xi'an Jiaotong University, Xi'an, 710049, China. ²Hysitron Incorporated, 10025 Valley View Road, Minneapolis, Minnesota 55344, USA. ³Department of Materials Science and Engineering, University of Pennsylvania, Philadelphia, Pennsylvania 19104, USA. ⁴Danish-Chinese Center for Nanometals, Materials Research Division, Risø National Laboratory for Sustainable Energy, Technical University of Denmark, DK-4000 Roskilde, Denmark. ⁵Department of Materials Science and Engineering, The Johns Hopkins University, Baltimore, Maryland 21218, USA.

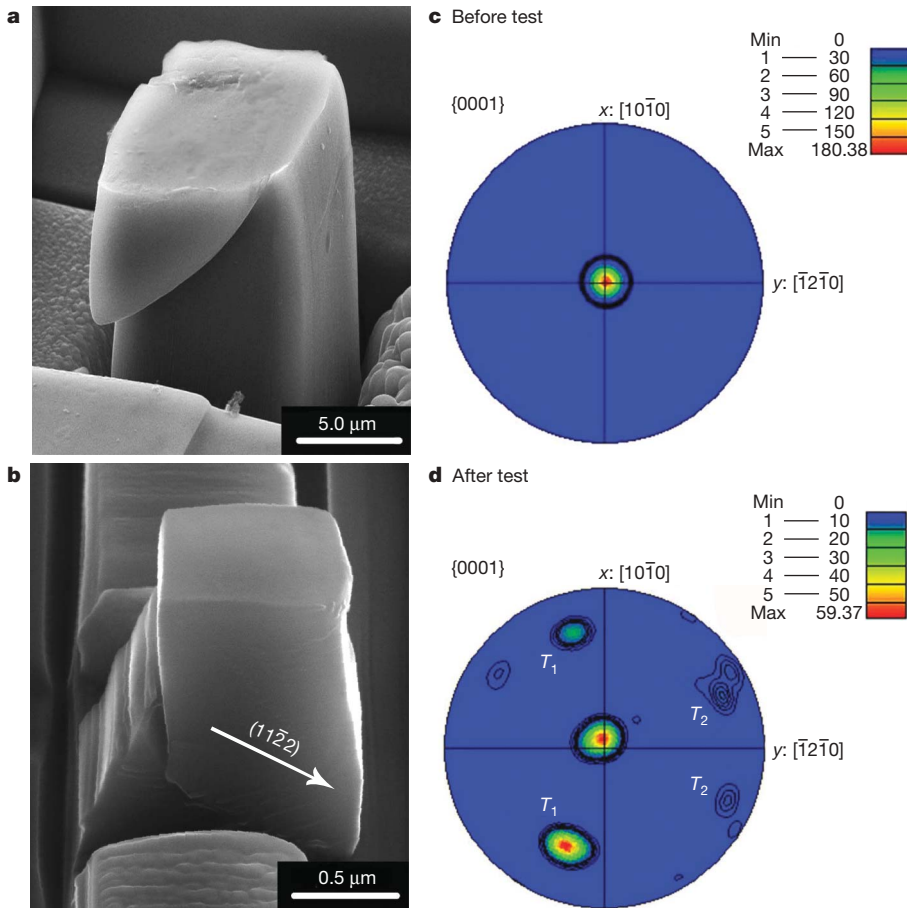


Figure 1 | Scanning electron microscopy images of the deformed micropillars and EBSD pole figure. **a**, $d = 8.0 \mu\text{m}$. **b**, $d = 1.0 \mu\text{m}$. **c**, **d**, EBSD pole figure of the $d = 8.0 \mu\text{m}$ pillar before (**c**) and after (**d**) compression. T_1 : $\{11\bar{2}2\}\langle\bar{1}\bar{1}23\rangle$ and T_2 : $\{10\bar{1}1\}\langle\bar{1}012\rangle$ denote the twin type. T_1 and T_2 have misorientation of $64^\circ/\langle 1\bar{1}00 \rangle$ and $57^\circ/\langle 2\bar{1}\bar{1}0 \rangle$, respectively, with respect to the initial orientation. (Half-width 10° ; cluster size 5° .)

and continuous plastic flow. TEM micrographs in Fig. 3c show that before the test, the density of dislocations is very low, except at the top of the pillar where a few dislocation lines were left from FIB damage (our TEM examinations indicate that the damage layer is only a few nanometres thick and should not affect the mechanism transition at the size scale of $d_c \approx 1 \mu\text{m}$). After the compression test, a high density of tangled dislocations is observed; see Fig. 3d. There is no sign of deformation twins from either the images or the diffraction patterns. The movie in the Supplementary Information, when correlated with Fig. 2c, reveals that during the first and second loading, only a few dislocations propagated from the contact surface into the pillar. The dislocation activities became intense only during the third loading, at which point the load reached $105 \mu\text{N}$ (the corresponding contact stress is $\sim 2 \text{ GPa}$, when dividing the load by the contact area). The continuous generation, multiplication and considerable accumulation of dislocations (see also Fig. 3d) are consistent with Fig. 2b and Fig. 2c: these submicrometre pillars exhibit smooth load-displacement curves in lieu of the large strain bursts corresponding to rapid deformation twin growth (Fig. 2a).

These results clearly demonstrate that deformation twinning is strongly dependent on the sample size. In micrometre-sized pillars, deformation twinning is still the dominant mode of plastic deformation, as in bulk-sized samples^{8,21–24}. As shown in Fig. 2d for the pillars with $d \geq 1 \mu\text{m}$, the strength (red symbols) and d (here the strength values are defined as the true stress measured at the twinning events, that is, the bursts in Fig. 2a) clearly follow a Hall–Petch-type relationship with $\alpha \approx 1$. We note that this strong size effect on deformation twinning is intrinsic to the material, because sample tapering is absent and the very thin FIB damage layer on the surface should be negligible in these relatively large samples.

At submicrometre sample sizes, in contrast, deformation twinning is suppressed, giving way to ODP only, even though our loading direction is favourable for deformation twinning. In addition, strain

bursts were not observed and the pillars were deformed into a mushroom-like geometry. For these submicrometre samples, we have defined the maximum flow stress as the peak load divided by the area of the narrowest cross-section $\pi d_{\text{narrowest}}^2/4$ of the mushroomed pillars (see inset in Fig. 2d) and plotted it in Fig. 2d. It is interesting to find that the maximum flow stress saturated at close to the material's ideal strength¹⁰, which is 2.8–4.9 GPa in pure shear for Ti⁹.

We wondered why deformation twinning follows a power-law scaling on d , and why $k_{\text{DT}} \gg k_{\text{ODP}}$. Here we present a ‘stimulated slip’ model to explain the size dependence of deformation twinning. In contrast to ODP, where inelastic shear activities are randomly dispersed among slip planes, deformation twinning is characterized by perfectly correlated layer-by-layer shearing: all slip (twinning dislocations) on atomically adjacent parallel planes must have the same Burgers vector. We posit that deformation twinning in relation to ODP is akin to what laser (light amplification by stimulated emission of radiation)²⁵ is to normal light, in the sense of slip coherence.

Here we consider a cuboidal crystal with size d and a total dislocation density ρ (in units of m^{-2}). These stored lattice dislocations may penetrate a twinning slip plane n of area d^2 (see Fig. 4). We assume that a small fraction P_{promoter} of the dislocations that penetrate plane n can play the role of ‘promoters’ (for example screw dislocations in various pole mechanisms^{2,6,26–28}), that ‘stimulate’ slip of the same character to occur also on the next atomic plane. Specifically, we assume that when a moving slip front (glide dislocation with twinning Burgers vector) on plane n hits and wraps around a promoter, inelastic shear of the same character ‘infects’ plane $n + 1$; and once infected anywhere on plane $n + 1$, we assume this stimulated twinning slip will propagate and cover the entire plane $n + 1$ as well, if the stress is high enough to drive it pass the forest dislocation obstacles, thickening the deformation twinning. The layer-to-layer ‘infection probability’ is simply

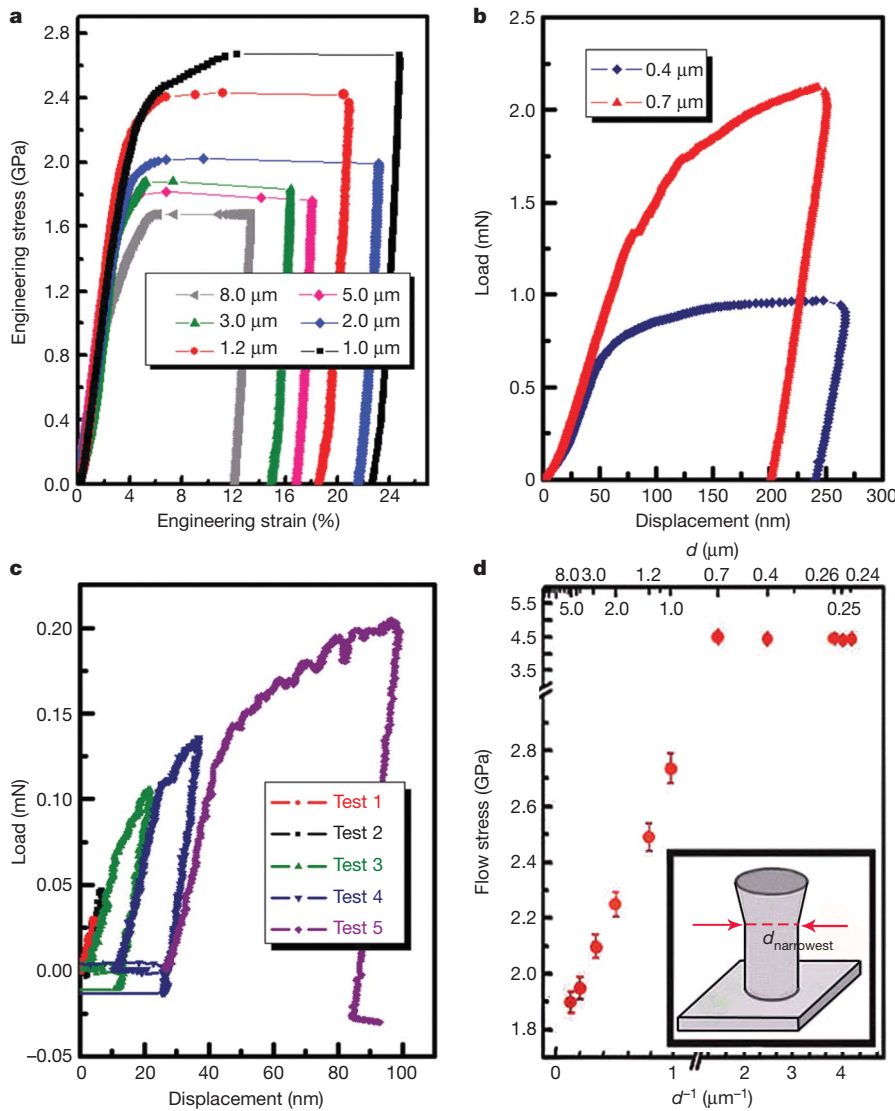


Figure 2 | Mechanical data of the tested samples. **a**, The stress–strain curves of micropillars with decreasing side length, d from 8.0 to 1.0 μm . **b**, The load–displacement curves of submicrometre pillars. **c**, The load–displacement curves of a submicrometre cylindrical pillar with 0.25 μm diameter, in five consecutive load–unload steps during *in situ* testing inside a TEM (see movie in the Supplementary Information). The negative forces at the end of the unloading segments are due to adhesion between diamond tip and the pillars. **d**, Flow stress measured for the pillars versus d . We use the narrowest cross-section $\pi d_{\text{narrowest}}^2/4$ to calculate the flow stress. The error bars are two standard deviations.

$$P_{\text{infection}} \approx d^2 \rho P_{\text{promoter}}$$

Deformation twinning keeps thickening when

$$1 \approx P_{\text{infection}}$$

and the critical dislocation density necessary for the sudden transition to perfect slip coherence is thus

$$\rho_c \approx d^{-2} P_{\text{promoter}}^{-1} \quad (3)$$

From the Taylor hardening model²⁹

$$\sigma = \sigma_0 + \kappa E b \rho^{1/2} \quad (4)$$

where E is the Young’s modulus, b is the Burgers vector length, κ is a dimensionless constant of order 1, σ_0 contains contributions from lattice friction, solute strengthening, and so on, we have the twinning stress

$$\sigma_{\text{DT}} = \sigma_0 + (\kappa E b P_{\text{promoter}}^{-1/2}) d^{-1} = \sigma_0 + k_{\text{DT}} d^{-1} \quad (5)$$

The best fit in Fig. 2d gives $\alpha = 0.976$, consistent with equation (5) above. The relatively large deformation twinning Hall–Petch slope k_{DT} (see also Supplementary Table 1 and ref. 18) can be explained by a

(1) small $P_{\text{promoter}} \approx 10^{-2}$, which is reasonable because only a small subset of the stored dislocations may be screw poles of the right type for promoting twinning slip. A full discussion of this model is provided in the Supplementary Information.

(2) A large k_{DT} in $\sigma_{\text{DT}} = \sigma_0 + k_{\text{DT}} d^{-1}$ drives early deformation-twinning abdicication ($d_c \approx 1 \mu\text{m}$), because as σ_{DT} approaches the ideal strength, there will be profuse dislocation nucleation, leading to high ODP strain rates. We note that as the pillars enter the submicrometre regime, the nucleation of ODP dislocations is increasingly assisted by the roughness left during FIB processing at the contact interface, and the now-very-large near-surface regions³⁰.

We conclude that deformation twinning is an intensely collective, ‘stimulated slip’ phenomenon, analogous to ‘stimulated emission’ in laser theory²⁵. Stimulated slip from plane n to plane $n + 1$ is catalysed by promoter defects, such as screw dislocation poles^{2,6,26–28}. Dual requirements must be met for deformation twinning: the stress needs to be high enough to drive a twinning dislocation to sweep plane n of area d^2 , cutting across forest obstacles; and of these forest obstacles, a sufficient proportion must be able to promote slip from plane n to $n + 1$. The smaller d is, the more weakly two adjacent slip planes are effectively coupled by threading screw pole dislocations, and the more difficult it is for deformation twinning. The large Hall–Petch slope k_{DT} implies a small promoter fraction P_{promoter} among the stored bulk dislocations, leading to a very large d_c , observed to be $\sim 1 \mu\text{m}$, at which Hall–Petch behaviour breaks down and transition to incoherent ODP occurs.

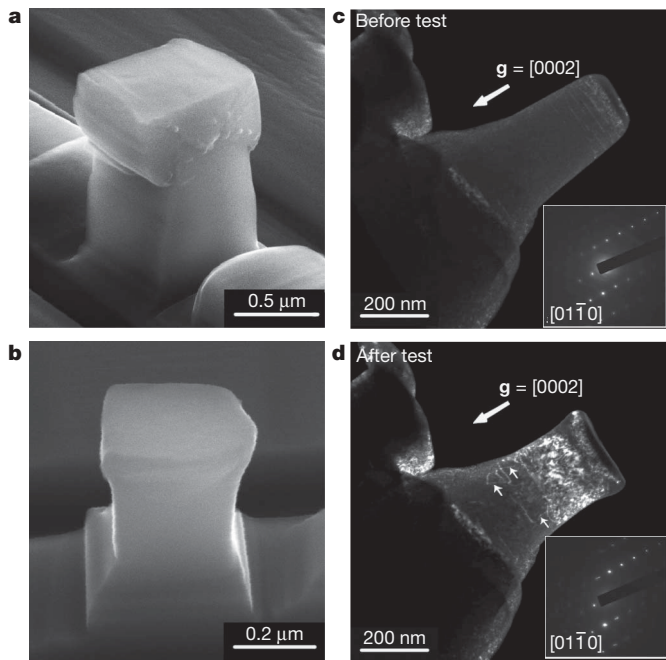


Figure 3 | Electron microscopy images of the tested samples. a, b, SEM images of the deformed $d = 0.7 \mu\text{m}$ (a) and $d = 0.4 \mu\text{m}$ (b) pillars. **c, d,** Centred dark-field TEM images with diffraction pattern (insets) of the $0.25\text{-}\mu\text{m}$ -diameter pillar before (c) and after (d) the *in situ* compression test. The beam direction was $[01\bar{1}0]$ and the reflection vector $\mathbf{g} = [0002]$.

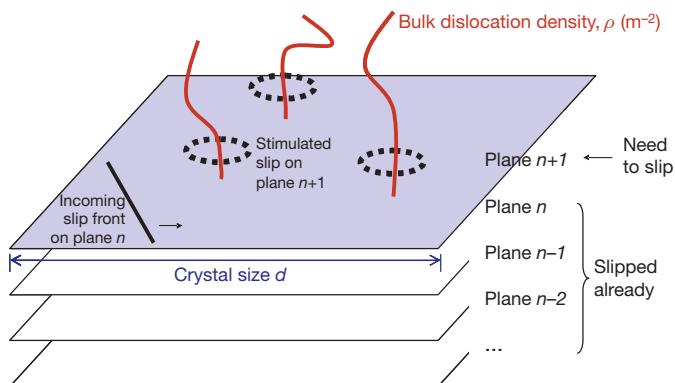


Figure 4 | Schematic of the 'stimulated slip' model. Thickening of deformation twin by 'stimulated slip' occurs when an incoming slip front (twinning glide dislocation) hits bulk screw dislocation 'promoters', a subset of the bulk forest dislocation population.

This size is of considerable technological importance. When the surface-bound contiguous crystal is reduced to the submicrometre scale, the effective interlayer coupling responsible for coherent 'stimulated slip' becomes so weak that deformation twinning is no longer triggered by bulk promoters, and incoherent ODP at high stress is sufficient to match the imposed strain rate. We note that the discussions above are based on a bulk promoter population, which scales with the volume. Deformation twinning proficiency may go up again at very small crystal sizes such as 10 nm (ref. 1), when the most effective promoters for stimulated slip may be grain boundaries and surfaces instead of screw dislocations, on the basis of an area-to-volume ratio argument.

METHODS SUMMARY

The orientation of the single crystal α -Ti alloy was determined using the Laue back reflection method. The pillar samples oriented along the c -axis for compression testing were prepared using FIB. Compression testing was performed using an MTS Nanoindenter XP and a Hysitron TEM PicoIndenter, respectively.

Received 13 July; accepted 17 November 2009.

- Chen, M. W. *et al.* Deformation twinning in nanocrystalline aluminum. *Science* **300**, 1275–1277 (2003).
- Christian, J. W. & Mahajan, S. Deformation twinning. *Prog. Mater. Sci.* **39**, 1–157 (1995).
- Ogata, S., Li, J. & Yip, S. Energy landscape of deformation twinning in bcc and fcc metals. *Phys. Rev. B* **71**, 224102 (2005).
- Wu, X. L. & Zhu, Y. T. Inverse grain-size effect on twinning in nanocrystalline Ni. *Phys. Rev. Lett.* **101**, 025503 (2008).
- Warner, D. H., Curtin, W. A. & Qu, S. Rate dependence of crack-tip processes predicts twinning trends in f.c.c. metals. *Nature Mater.* **6**, 876–881 (2007).
- Niewczas, M. in *Dislocations in Solids* Vol. 13 (eds Nabarro, F. R. N. & Hirth, J. P.) 263–364 (Elsevier, 2007).
- Song, S. G. & Gray, G. T. Structural interpretation of the nucleation and growth of deformation twins in Zr and Ti. *Acta Metall. Mater.* **43**, 2325–2350 (1995).
- Williams, J. C., Baggerly, R. G. & Paton, N. E. Deformation behavior of HCP Ti-Al alloy single crystals. *Metall. Mater. Trans. A* **33**, 837–850 (2002).
- Ogata, S., Li, J., Hirotsuki, N., Shibutani, Y. & Yip, S. Ideal shear strain of metals and ceramics. *Phys. Rev. B* **70**, 104104 (2004).
- Suresh, S. & Li, J. Deformation of the ultra-strong. *Nature* **456**, 716–717 (2008).
- Lu, L., Chen, X., Huang, X. & Lu, K. Revealing the maximum strength in nanotwinned copper. *Science* **323**, 607–610 (2009).
- Argon, A. S. & Yip, S. The strongest size. *Phil. Mag. Lett.* **86**, 713–720 (2006).
- Schiotz, J. & Jacobsen, K. W. A maximum in the strength of nanocrystalline copper. *Science* **301**, 1357–1359 (2003).
- Shan, Z. W. *et al.* Grain boundary-mediated plasticity in nanocrystalline nickel. *Science* **305**, 654–657 (2004).
- Uchic, M. D., Dimiduk, D. M., Florando, J. N. & Nix, W. D. Sample dimensions influence strength and crystal plasticity. *Science* **305**, 986–989 (2004).
- Shan, Z. W., Mishra, R. K., Asif, S. A. S., Warren, O. L. & Minor, A. M. Mechanical annealing and source-limited deformation in submicrometre-diameter Ni crystals. *Nature Mater.* **7**, 115–119 (2008).
- Greer, J. R., Oliver, W. C. & Nix, W. D. Size dependence of mechanical properties of gold at the micron scale in the absence of strain gradients. *Acta Mater.* **53**, 1821–1830 (2005).
- Meyers, M. A., Vohringer, O. & Lubarda, V. A. The onset of twinning in metals: a constitutive description. *Acta Mater.* **49**, 4025–4039 (2001).
- Stanford, N., Carlson, U. & Barnett, M. R. Deformation twinning and the Hall-Petch relation in commercial purity Ti. *Metall. Mater. Trans. A* **39**, 934–944 (2008).
- El-Danaf, E., Kalidindi, S. R. & Doherty, R. D. Influence of grain size and stacking-fault energy on deformation twinning in fcc metals. *Metall. Mater. Trans. A* **30**, 1223–1233 (1999).
- Paton, N. E. & Backofen, W. A. Plastic deformation of titanium at elevated temperatures. *Metall. Trans.* **1**, 2839–2847 (1970).
- Akhtar, A. Basal slip and twinning in alpha-titanium single-crystals. *Metall. Trans. A* **6**, 1105–1113 (1975).
- Yoo, M. H. Twinning and mechanical behavior of titanium aluminides and other intermetallics. *Intermetallics* **6**, 597–602 (1998).
- Xiao, L. Twinning behavior in the Ti-5 at.% Al single crystals during cyclic loading along. *Mater. Sci. Eng. A* **394**, 168–175 (2005).
- Svelto, O. *Principles of Lasers* (Springer, 1998).
- Cottrell, A. H. & Bilby, B. A. A mechanism for the growth of deformation twins in crystals. *Phil. Mag.* **42**, 573–581 (1951).
- Niewczas, M. & Saada, G. Twinning nucleation in Cu-8 at.% Al single crystals. *Phil. Mag. A* **82**, 167–191 (2002).
- Song, S. G. & Gray, G. T. Double dislocation pole model for deformation twinning in fcc lattices. *Phil. Mag. A* **71**, 661–670 (1995).
- El-Azab, A. The statistical mechanics of strain-hardened metals. *Science* **320**, 1729–1730 (2008).
- Zhu, T., Li, J., Samanta, A., Leach, A. & Gall, K. Temperature and strain-rate dependence of surface dislocation nucleation. *Phys. Rev. Lett.* **100**, 025502 (2008).

Supplementary Information is linked to the online version of the paper at www.nature.com/nature.

Acknowledgements We thank Q. Liu for help with EBSD experiments. This work was supported by grants from the NSFC (50671077, 50720145101, 50831004 and 50925104), the 973 Program of China (2004CB619303, 2007CB613804 and 2010CB613003) and the 111 Project of China (B06025). J.L. was supported by ONR grant N00014-05-1-0504, NSF grant CMMI-0728069, MRSEC grant DMR-0520020 and AFOSR grant FA9550-08-1-0325. X.H. was supported by the Danish National Research Foundation. The *in situ* TEM work was performed at the National Center for Electron Microscopy, Lawrence Berkeley Laboratory, which is supported by the US Department of Energy under contract DE-AC02-05CH11231.

Author Contributions Q.Y. and Z.-W.S. carried out the experiments, J.L. constructed the model, X.H. interpreted the EBSD results, L.X. supervised the sample selection, J.S. designed the project, J.L. and E.M. wrote the paper. All authors contributed to the discussions.

Author Information Reprints and permissions information is available at www.nature.com/reprints. The authors declare no competing financial interests. Correspondence and requests for materials should be addressed to J.S. (junsun@mail.xjtu.edu.cn) or J.L. (liju@seas.upenn.edu).

A simple schematic that summarizes the main finding of our paper is Fig. S1.

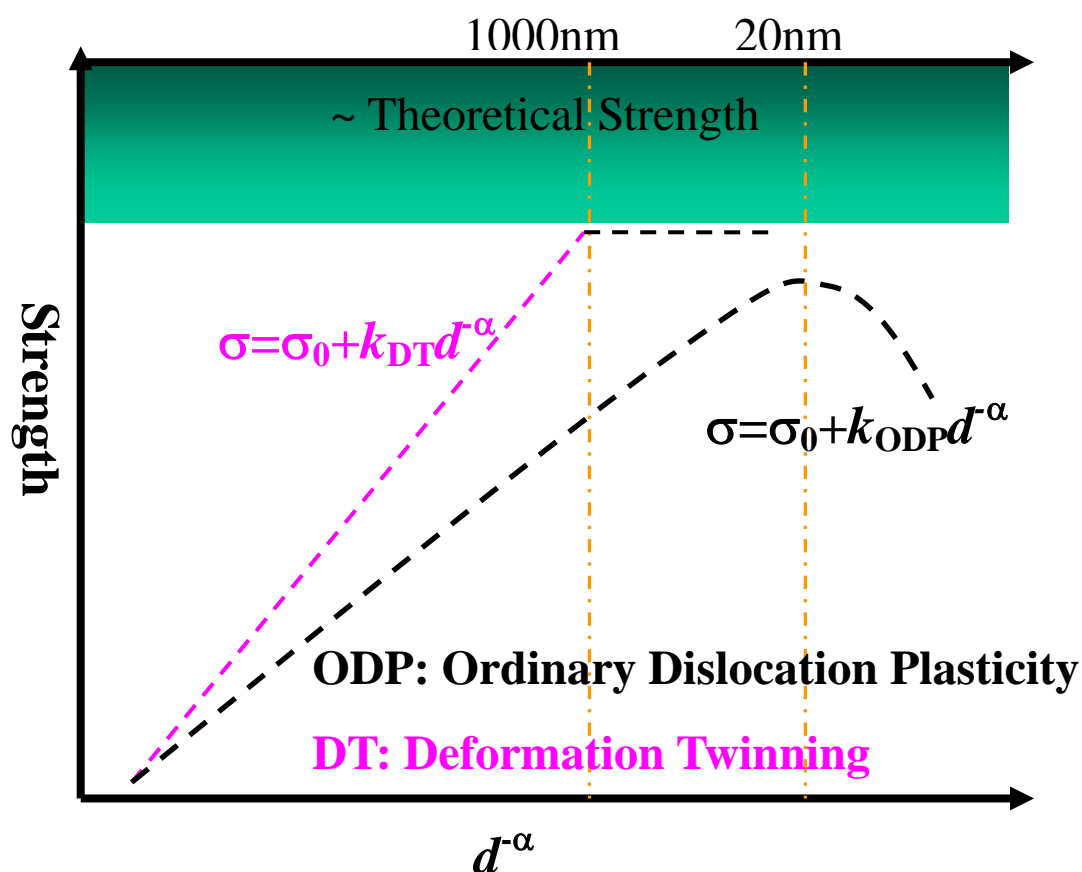


FIG S1: Comparison of Hall-Petch scaling and Hall-Petch breakdown between ordinary dislocation plasticity (ODP, black curve)¹⁻³ and deformation twinning (DT, magenta curve). Deformation twinning is much more size aware than ordinary dislocation plasticity in BCC and HCP metals, as indicated in Table S1 for the *grain size* dependence.

Table 1. Comparison of Hall–Petch slopes for slip and twinning

Material	H–P slope for slip k_S (MPa mm ^{1/2})	H–P slope for twinning k_T (MPa mm ^{1/2})
<i>BCC</i>		
Fe–3 wt%Si (Hull)	10.4 (RT) 17.64 (77 K)	38.48
Fe–3 wt%Si (Loeche and Vöhringer)	12	100
ArmcoFe (Loeche and Vöhringer)	20	124
Armco Fe (Moiseev and Trefilov)		90
Steels: 1010, 1020, 1035 (Loeche and Vöhringer)	20	124
Fe–25at%Ni (BCC) (Nilles and Owen)	33	100
Cr (Marcinkowski and Lipsitt)	10.08	67.75
Va (Lindley and Smallman)	3.46 (20 K)	22.37
<i>FCC</i>		
Cu (Vöhringer)		21.6 (77 K)
(Meyers et al.)	5.4 (RT)	
(Zerilli and Armstrong)	5.2 (RT)	
Cu–6 wt%Sn	7.1	11.8 (77 K)
Cu–9 wt%Sn	8.2	7.9 (295 K)
Cu–10 wt%Zn	7.1	15.7 (77 K)
Cu–15 wt%Zn (Vöhringer; Koester and Speidel)	8.4	11.8 (77 K) 16.7 (295 K)
<i>HCP</i>		
Zr (Song and Gray)	8.25	79.2
Ti (Okazaki and Conrad)	6 (78 K)	18 (4 K)

Table S1: Taken from Meyers, M. A., Vohringer, O., Lubarda, V. A., “The onset of twinning in metals: A constitutive description,” *Acta Mater.* 49 (2001) 4025, for *grain size* effect on deformation twinning.

1. Methods

The crystal orientation of the Ti-5at%Al single crystal was determined using the Laue back reflection method. A group of micron and submicron pillar samples oriented along the c -axis for compression testing were prepared using the Focused Ion Beam (FIB) micromachining technique⁴. The samples have square cross-sections with the side length (d) in the range of 8.0 to 0.4 μm , and an aspect ratio of $\sim 2:1$. Two orthogonal faces, which were used for surface trace analysis, were made to be parallel to the $(10\bar{1}0)$ plane and the $(1\bar{2}10)$ plane, respectively. In addition, cylindrical pillars with a diameter of about 250 nm were fabricated by FIB cutting, using the method described by Shan et al.⁵. All the samples have their long (height) axis parallel to the $[0001]$ direction (this orientation was confirmed to remain unchanged after testing).

Compression testing was performed using an MTS Nanoindenter XP, outfitted with a flat-tip diamond punch, at a nominal axial strain rate of $5 \times 10^{-4}/\text{s}$ to $1 \times 10^{-4}/\text{s}$ at room temperature. For micro-pillars with $d > 1 \mu\text{m}$, electron backscatter diffraction (EBSD) with a step size of 50 nm in a field-emission scanning electron microscope (SEM) was used to investigate the evolution of the microstructure (such as the orientation of the twins) in the deformed samples. TEM samples were prepared using FIB, for microstructural observation in a JEOL 2100F microscope. The centered dark field TEM images presented were not taken under strict weak-beam conditions, due to the limited tilting capability available inside the holder. For the 250 nm samples, *in situ* nano-compression experiments were carried out at room temperature in a JEOL 3100 TEM operating at 300kV, employing a Hysitron TEM PicoIndenter⁵; this test directly correlates the microstructural evolution with the mechanical data throughout the test.

Movie of the *in situ* compression of the 250 nm Ti-5at%Al single crystal pillar in TEM is placed at *Nature* website.

2. Deformation Twinning in Bulk Ti-5%Al

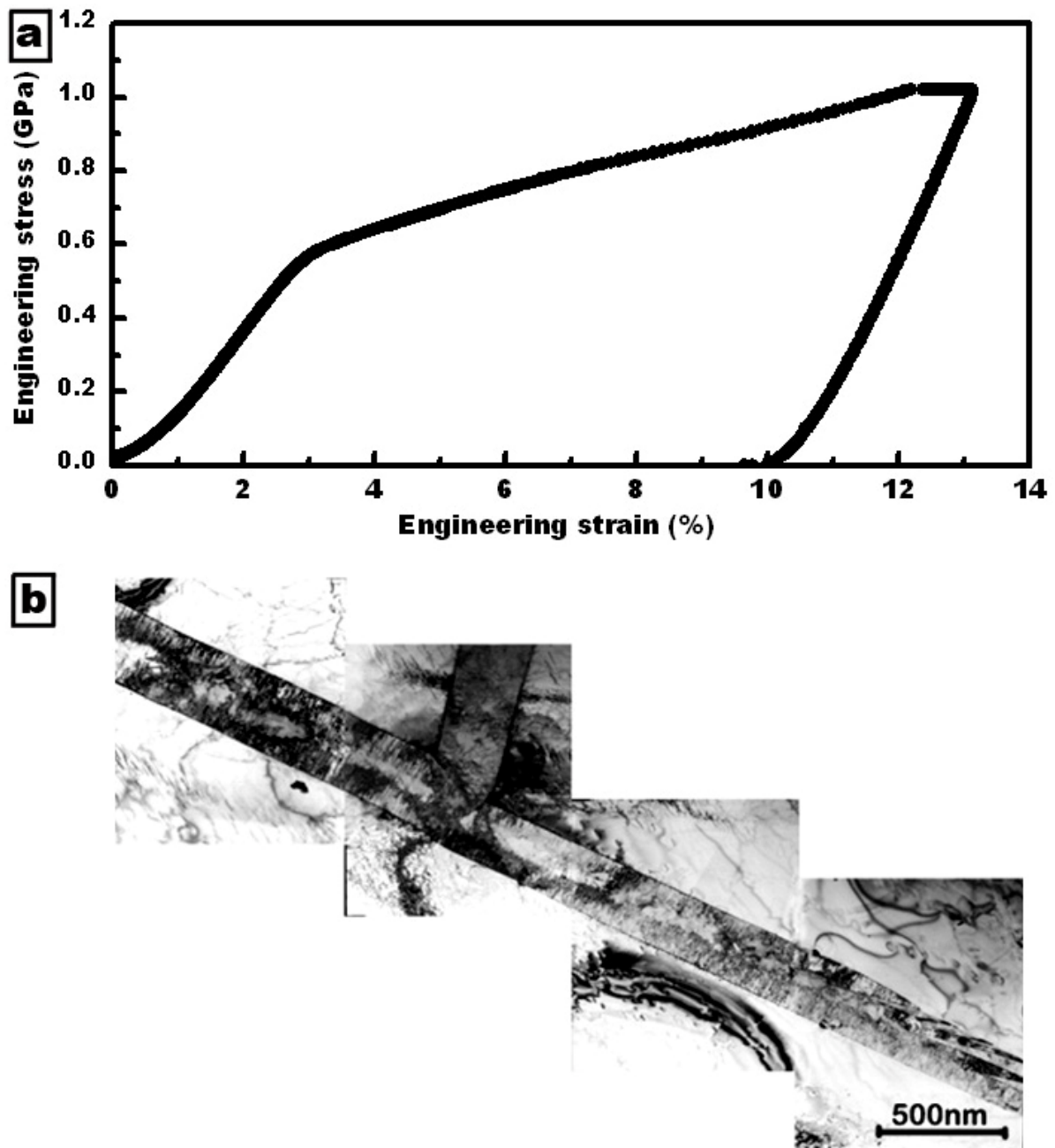


FIG S2: (a) Engineering stress-strain curve and (b) TEM micrographs of Ti-5at%Al single crystal loaded in the [0001] direction. The sample in (a) has dimensions 3 mm×3 mm×6 mm. Note the typical dimensions and morphologies of the deformation twins in (b).

3. TEM Characterization of Deformed Ti-5%Al Micropillars

We have carried out transmission electron microscopy characterizations of the deformed pillars. The TEM slab specimens were cut using focused ion beam. Details of the sample preparation procedures are illustrated in Fig. S3. The results, shown below in Fig. S4 and Fig. S5 as examples, indicate that deformation twinning indeed occurs in the midst of lattice dislocations in $d > d_c$ pillars. A typical example showing multiple deformation twins is given in Fig. S4A which is a centered dark field TEM image. The diffraction spots from the matrix and those from the twins are marked with blue and green line, respectively in the corresponding selected area diffraction pattern (Fig. S4B). The diffraction spot used for imaging Fig. S4A is indicated by the short green arrow in Fig. S4B. From these, some of the twins can be identified as of the $\{10\bar{1}1\}\langle\bar{1}012\rangle$ type.

It is worth noting that the twins with smaller sizes, i.e. twin embryos, exhibit convex lens shape. This is in contrast to those observed in their bulk counterpart where the twin boundaries are usually straight and long (Fig. S2b). The deformation twin embryos are indeed located in a region of high dislocation densities (Fig. S5). The majority of the dislocation segments are of edge character. However, the ledges associated with the long dislocation lines and the bowing-out ends of dislocations in the tangled dislocations are screw segments, prerequisite for the pole mechanism. From $\mathbf{g}\cdot\mathbf{b}$ analysis, we have found dislocations with Burgers vectors of all the three major types, $\langle\mathbf{a}\rangle$, $\langle\mathbf{c}\rangle$ and $\langle\mathbf{a}+\mathbf{c}\rangle$.

When $d > d_c$ (micrometer sized) pillars are deformed plastically but are cut open prior to strain burst in the stress vs. strain curve, TEM analyses show dislocation conformation and density similar to Fig. S5, but no twins. These results provide the experimental evidence of the prior occurrence of ordinary dislocation plasticity (ODP, “incoherent slip”) and dislocation density storage as a prerequisite for the initiation of deformation twinning (“coherent slip”). It is also consistent with the other results in several respects. First, the stress vs. strain (load vs. displacement) curves (Fig. 2a & Fig. S2a) clearly showed that considerable ODP, which gives

smooth flow, occurred prior to the strain bursts (twin initiation). Second, post mortem TEM observations in a deformation twinning dominated sample confirmed the existence of a large number of dislocations besides the deformation twins (Fig. S2b). Third, *in situ* TEM compression tests showed the prevalence of dislocation activity in the absence of deformation twinning (see movie at *Nature* website). The observed curved dislocation tangles include many dislocation segments with screw character.

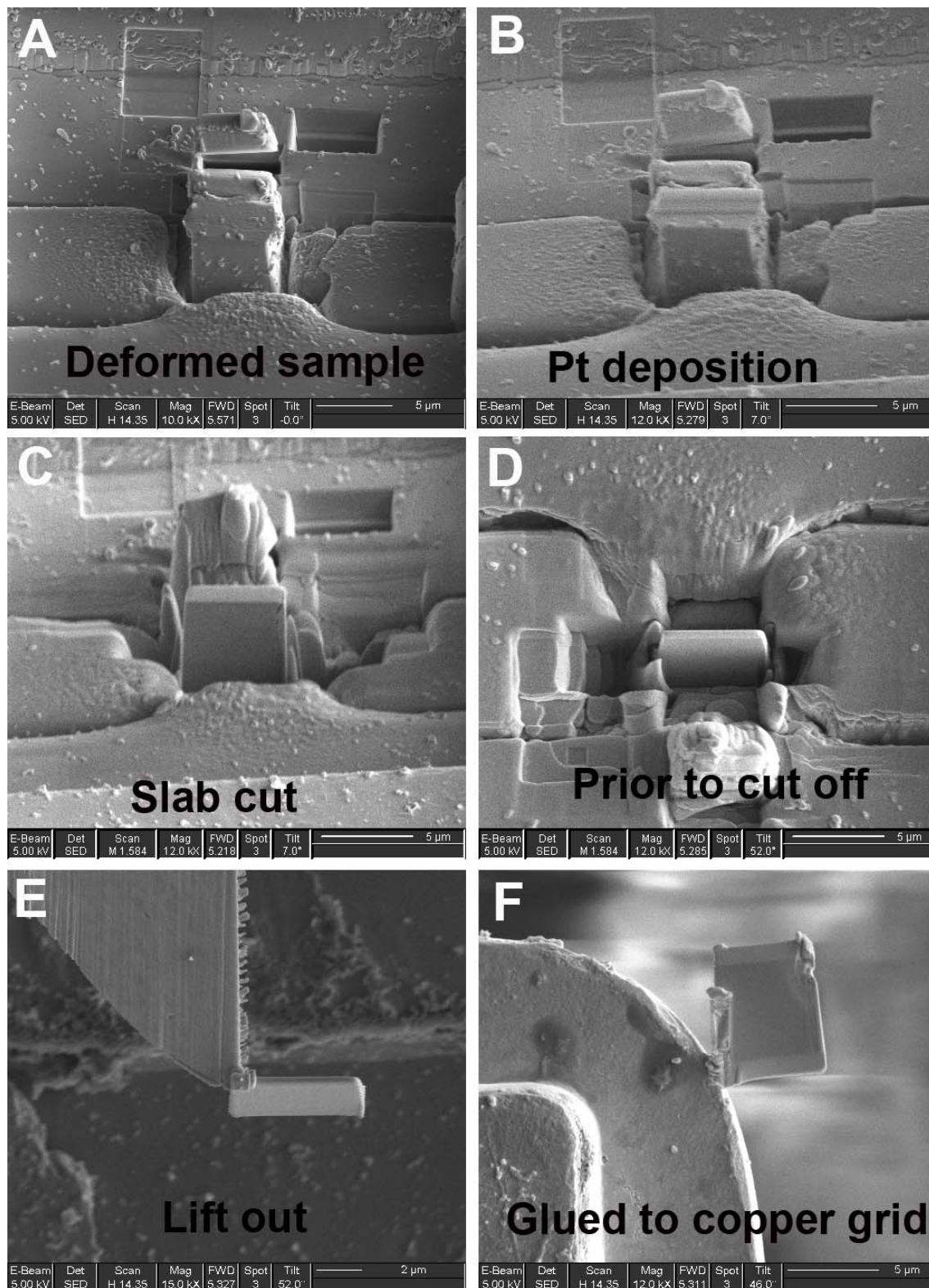


Fig. S3: Cross-section-view TEM sample preparation of a deformed pillar with $0.8 \mu\text{m}$ diameter. (A) deformed sample; (B) A layer of Pt was deposited on top of the deformed pillar; (C) A thin slab of sample was cut with focused ion beam; (D) e-beam image of the slab prior to be cut off; (E) Sample lift out; (F) Sample was glued to an Omniprobe grid for further thinning.

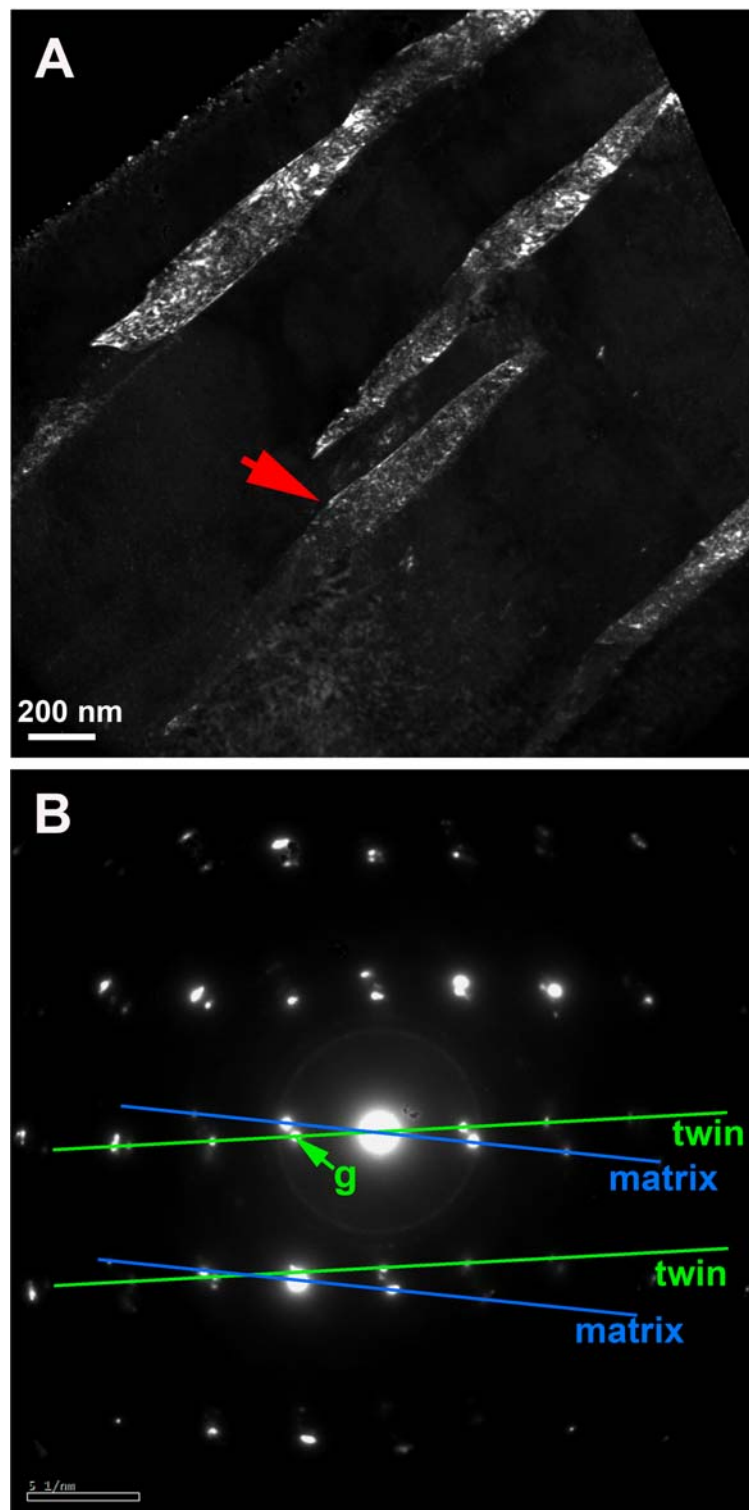


Fig. S4: Deformation twins in the deformed pillar in Fig. S3. (A) is a typical dark field TEM image of deformation twins. Note the smaller twin indicated by the short red arrow exhibit a convex lens shape. (B) is the corresponding selected area diffraction pattern of (A). The blue and green lines mark the diffraction spots from the matrix and the twin, respectively. The diffraction vector used to image (A) was highlighted with the green arrow in (B).

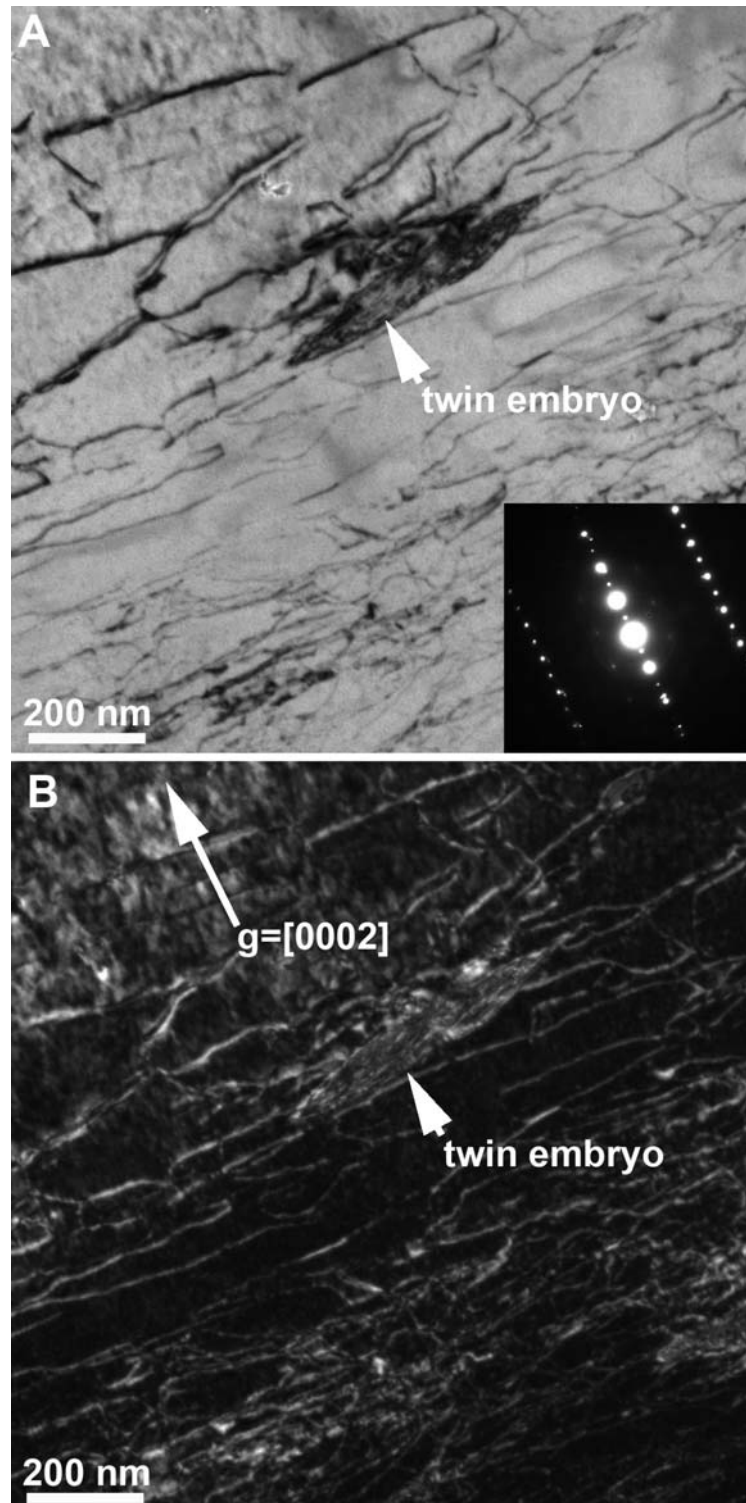


Fig. S5: Twin embryo observed in a matrix of dislocations. (A) and (B) are bright field and centered dark field TEM images, respectively. The inset in (A) is the corresponding selected area diffraction pattern. The twin embryo (white arrow in both A and B) exhibited typical convex lens shape. The diffraction vector used for imaging was $g=[0002]$.

4. A “Stimulated-Slip” Model for Size-Dependent Deformation Twinning

Deformation twinning (DT) is a highly correlated atomic shearing process⁶, which we deduce in the model below to arise out of ODP (ordinary dislocation plasticity) but then supercedes ODP if $d > d_c$. In the model below, we will employ the analogy that DT versus ODP is like what laser (Light Amplification by Stimulated Emission of Radiation) is to normal light. To begin, let us consider a cuboidal crystal volume consisting of m slip planes, say $m = 10,000$. If this crystal volume sustains a plastic shear strain of 1%, it would mean 100 planes have slipped. If this occurred by ODP, it is likely that the 100 slipped planes are nearly randomly dispersed among the 10,000, which means that on average $\sim 10^2$ planes separate one slipped plane from the next closest slipped plane. This means the probability that the two slipped planes are situated right next to each other is very small. If so, slip activities on the two planes are unlikely to be strongly correlated. In contrast, if the 1% plastic strain is accomplished by DT, then it is very likely that tens, or even the entire 100, slipped planes are adjacent right next to each other, in blocks. In many experiments it is not difficult to see micrometer-thick deformation twins. This means that for DT the average distance between one slipped plane and the next closest slipped plane will be close to 1 atomic layer spacing, whereas it is $\sim 10^2$ in ODP. Therefore, slip activities are much more strongly correlated in DT than in ODP, on parallel planes at the atomic level. This has an underlying atomic energetics reason⁶. What is intriguing, however, is that the propensity for DT versus ODP also depends on the crystal volume, i.e., the size effect. Our experiments indicate that the larger the contiguous crystal volume, the perfectly coherent DT mode is more favored over the less collective, incoherent ODP mode.

Another intriguing fact is that while DT and ODP are both found experimentally to follow a Hall-Petch type size-dependent strengthening behavior: $\sigma = \sigma_0 + kd^{-\alpha}$, DT has much larger Hall-Petch slope than ODP: $k_{DT} \gg k_{ODP}$ in many materials, sometimes by an order of magnitude⁷, for the same α . This means DT is even more size-aware than ODP. Such rapid rise in flow stress with shrinking size means the breakdown of DT Hall-Petch scaling relation must occur at a much larger critical size d_c than what is typically expected for ODP (~ 20 nm)

^{2,3,8}. When one uses the ideal shear strength of pure Ti (calculated from density functional theory to be 2.8-4.9 GPa⁹) as an upper bound for σ , and k_{DT} measured from μm -sized Ti alloy crystals, one anticipates a DT Hall-Petch breakdown d_C from several hundred nms to 1 μm , a much more conspicuous and experimentally accessible (and engineering-wise important) sizescale than the $d_C \sim 20\text{nm}$ for the ODP-grain boundary sliding transition in nanocrystals ^{2,3,10}.

Since the large d_C for DT is tied to its large k_{DT} , the key to understanding the Hall-Petch behavior and its breakdown is answering:

- (a) What physical mechanism drives $\sigma = \sigma_0 + kd^\alpha$ behavior for deformation twinning?
- (b) Why is k_{DT} so large?

We believe both (a) and (b) can be satisfactorily answered by inspecting the highly correlated, “stimulated slip” nature of deformation twinning.

We hypothesize that when slip progresses on one atomic plane n , there can be certain “promoter” defects such as screw dislocations, grain boundaries, and others, that can promote slip of *identical* character to also occur on plane $n+1$, parallel and immediately adjacent to plane n . This is termed “stimulated slip” here, analogous to the concept of “stimulated emission” in laser theory¹¹. The idea is that there is an enhanced probability of having slip of the same character (same Burgers vector) to also occur on plane $n+1$, above and beyond the average probability of having “spontaneous slip” on plane $n+1$ from ODP, if (i) the atomic plane n is undergoing slip of this Burgers vector, and (ii) plane n intersects a promoter defect. Classic examples of promoter defect and “stimulated slip” are various kinds of pole mechanisms^{7,12-14}. Although details vary, the common key element of pole mechanisms is bulk screw dislocation(s) intersecting the twinning glide plane. The screw dislocation(s) warps originally disjoint parallel slip planes into a continuous staircase helix, such that slip can propagate up or down the staircase. One can also envision various kinds of rebound

mechanisms¹⁵ occurring at the boundary of a crystal volume. For instance, in a FCC crystal when one Shockley partial dislocation hits a grain boundary or free surface, there can be enhanced probability that another Shockley partial emerges at the locale of the hit, but on one plane above or below, which will then move backward and proceed to thicken the deformation twin. These detailed mechanisms can be modeled atomistically to high accuracy^{16,17}. One however could proceed with the generic concept of “promoter” defects and “stimulated slip” to obtain size-dependent DT behavior, without specifying the detailed atomistic mechanisms.

Next, we examine the consequence of a *bulk* “promoter” defect population on the size scaling of DT, specifically pole mechanisms requiring bulk screw dislocations, which are part of the general dislocation population characterized by the total dislocation density ρ (unit $1/\text{m}^2$). While *boundary* “promoters” such as grain boundary or free surfaces are likely to become important at size scales of tens of nanometers and below¹⁸, we suggest that boundary “promoters” are less important in our present experiments dealing with characteristic dimensions near $1\ \mu\text{m}$, based on a area-to-volume ratio argument.

In Fig. 4 illustration of the main text, we presume stimulated slip has already occurred on planes $n-1$, $n-2$, ... and is sweeping on plane n . Since the size scale of the contiguous crystal volume is d , planes n , $n-1$, $n-2$, ... all have area $\sim d^2$. Here, it is important to appreciate the way size d^2 comes into the problem. Like laser, deformation twinning requires *perfect coherence* in slip activities, i.e. slip on plane n , $n-1$, $n-2$, ... must all have the same Burgers vector. Suppose our contiguous crystal volume is bounded by grain boundaries, when stimulated slip hits a grain boundary this perfect coherence must be heavily disrupted. This is because the adjacent grain is misoriented with respect to our grain, with non-parallel, intersecting slip planes, so slip *must* change character even if it wants to proceed onto the next grain. Furthermore, grain boundaries have larger CSL-period (coincident site lattice) or even random structures, which will also heavily disrupt the perfect slip coherence. Therefore, the area-wise extent of perfect slip coherence is likely bounded by d^2 . The key to the survival of the deformation twinning mode is whether perfect slip coherence can be sustained in the

thickness direction. In order to achieve this, the one-layer-to-next-layer “infection probability” $P_{\text{infection}}$ must be nearly 100%. That is to say, conditional upon plane n is slipping and plane $n+1$ has not yet slipped, the probability that plane $n+1$ will get “infected” to slip in the same way (stimulated slip) must be nearly 1, in order to achieve runaway propagation of perfect slip coherence in the thickness direction. Otherwise, one cannot possibly see deformation twins microns thick in experiments, involving thousands of consecutive atomic planes.

In our simple model, we assume that a fraction P_{promoter} ($0 < P_{\text{promoter}} < 1$) of the total dislocation population act as promoter dislocations. We also assume that when the slip sweeps on plane n , if it hits a forest dislocation that penetrates the plane, which turns out to be a promoter, inelastic shear of the same character will infect plane $n+1$. Once infected anywhere on plane $n+1$, of area d^2 , this stimulated slip will eventually propagate and cover the entire d^2 area at some speed. Thus, the one-layer-to-next-layer “infection probability” is simply

$$P_{\text{infection}} = d^2 \rho P_{\text{promoter}} . \quad (1)$$

In order to trigger perfectly coherent DT, there needs to be

$$1 \approx P_{\text{infection}} . \quad (2)$$

According to (1),(2), if one starts deformation on a well-annealed sample with low ρ , DT must be preceded by ODP activities, working like an optically-pumped laser. The temporal sequence would be the following. In experiments where stress is ramped up from zero, there are always some ODP activities even at the beginning. It is just that these ODP dislocations have high core energy and/or low mobility and/or low Schmid factors, such that their strain rate contribution cannot match the applied strain rate at low stresses. This difference in strain rates gets accumulated to the elastic strain and causes the stress σ to rise. However, before the stress σ rises to high enough levels to allow sufficient ODP to accommodate all the strain rate imposed, the ODP dislocations “catch fire and start lasing” (DT). Once the highly

correlated DT mode is established, it is fast and efficient, and can match whatever applied strain rate that is given⁶. This is presumably what happens at $d > d_c$.

The size scaling of DT stress can now be derived, since it is just the critical ODP stress where runaway condition (see Eqs. (1) and (2) above) for the transition to perfect coherence is satisfied. For the ODP flow stress, we have the familiar Taylor model:

$$\sigma = \sigma_0 + \kappa E b \rho^{1/2} \quad (3)$$

where E is the Young's modulus, b is Burgers vector length, κ is a dimensionless constant of order 1. σ_0 contains contributions from lattice friction, solute strengthening, etc. From Eqs. (1) and (2), we see that the sudden transition to perfect slip coherence occurs at a critical dislocation density

$$\rho_c = d^2 P_{\text{promoter}}^{-1} \quad (4)$$

Thus, we obtain:

$$\sigma_{\text{DT}} = \sigma_0 + (\kappa E b P_{\text{promoter}}^{-1/2}) d^1 = \sigma_0 + k_{\text{DT}} d^1 \quad (5)$$

Eq. (5) answers the two key questions we raised at the beginning:

(a) DT has Hall-Petch like size scaling, with Hall-Petch exponent 1 by our simple model.

This arises because of the necessity to sustain perfect slip coherence in the thickness direction. Forest dislocations of screw character can thread adjacent slip planes together and promote stimulated slip, and the larger the area, the more likely the two adjacent planes are effectively coupled, until a critical condition is reached where perfect slip coherence can be sustained. As the limiting cases, DT always happens if d is sufficiently large, even for small ρ and P_{promoter} , and conversely, DT can be suppressed altogether at small enough d , for any reasonable ρ and P_{promoter} .

(b) k_{DT} is so large because P_{promoter} is small. $\kappa E b$ in (5) are the usual normalization

constants from ODP, and can be regarded as 1 in reduced units: in order for $k_{DT} \gg k_{ODP}$ by a factor of 10, as seen in many metals⁷, the magnitude of $P_{promoter}$ should be $\sim 10^{-2}$. This is reasonable, because only a small fraction of the stored forest dislocations can serve as effective promoters for twinning slip in pole mechanisms^{7,12-14}. By our model, only 1% of the stored forest dislocations that penetrate the twinning system glide planes are operative “helical staircases” that can promote stimulated slip on the next plane.

Note that equation (5) comes from a very simple model. It is implicitly assumed that the in-plane slip propagation is very easy, and coherence can be maintained in an entire d^2 area once started. Also, $P_{promoter}$ is assumed to be a constant with no stress dependence. Once these complexities are taken into account, it is likely that the best-fit Hall-Petch exponent could deviate from 1. Nonetheless, our simple model can already address the key questions underlying the DT size dependence, and illustrate the nature of DT as a perfectly correlated, stimulated slip phenomenon catalyzed by promoter defects.

Because of the large Hall-Petch slope $k_{DT} = \kappa E b P_{promoter}^{-1/2}$, the Hall-Petch scaling for DT $\sigma_{DT} = \sigma_0 + k_{DT} d^1$ would hit the ultra-strength regime^{19,20} at a conspicuously large and experimentally easily accessible d , and must therefore break down, because strain rate would diverge to infinity when one approaches the ideal shear strength. For $d < d_c$, the ODP dislocations never manage to “catch fire and start lasing” (DT), because adjacent slip planes are weakly effectively coupled due to small d^2 . In stress-ramp-up experiments, the stress σ will manage to rise high enough to drive an ODP-mediated strain rate that matches the applied strain rate, and reach steady-state flow, before it can reach the coherence transition. The DT mechanical energy dissipation channel never gets activated, and the ODP dissipation channel becomes the primary one throughout the loading path. In our analogy, the system is then just an ordinary light bulb, not an optically-pumped laser¹¹.

Finally, we would like to remark that the discussions above are based on a bulk promoter population whose total number scales with the volume. DT proficiency may go up again over

a range of very small crystal sizes, such as 10 nm¹⁸, when the most effective promoters for stimulated slip are GBs and surfaces instead of screw dislocations. This is beyond what we have discussed in the paper. Based on an area-to-volume ratio argument, the promotion efficacy of GBs/surfaces may exceed that of the bulk at very small crystal sizes, for emitting the “right” sequence of partial dislocations for DT. Indeed, Chen et al. have argued that for Al with high stacking-fault energy there can be *some* DT in very small nanograins, as the partial dislocations get emitted more easily from the GBs at tiny grain sizes¹⁸. So the observation of DT in nano-grains is not inconsistent with this paper, just at a very different size regime. Also, unlike the bulk promoter case presented here, where DT dominance in terms of contribution to the plastic strain at $d > 1\mu\text{m}$ is clearly affirmed from the stress-strain curves, in nanograined Al although deformation twins are observed in TEM, it is uncertain that DT has contributed more to the net plastic strain than ODP or grain boundary sliding – i.e. DT *dominance* was not affirmed as a *regime* in nanocrystalline Al.

References

1. Lu, L., Chen, X., Huang, X. & Lu, K. Revealing the Maximum Strength in Nanotwinned Copper. *Science* **323**, 607-610 (2009).
2. Argon, A. S. & Yip, S. The strongest size. *Philosophical Magazine Letters* **86**, 713-720 (2006).
3. Schiotz, J. & Jacobsen, K. W. A maximum in the strength of nanocrystalline copper. *Science* **301**, 1357-1359 (2003).
4. Uchic, M. D., Dimiduk, D. M., Florando, J. N. & Nix, W. D. Sample dimensions influence strength and crystal plasticity. *Science* **305**, 986-989 (2004).
5. Shan, Z. W., Mishra, R. K., Asif, S. A. S., Warren, O. L. & Minor, A. M. Mechanical annealing and source-limited deformation in submicrometre-diameter Ni crystals. *Nature Materials* **7**, 115-119 (2008).
6. Ogata, S., Li, J. & Yip, S. Energy landscape of deformation twinning in bcc and fcc metals. *Physical Review B* **71**, 224102 (2005).
7. Meyers, M. A., Vohringer, O. & Lubarda, V. A. The onset of twinning in metals: A constitutive description. *Acta Mater.* **49**, 4025-4039 (2001).
8. Yip, S. Nanocrystals - The strongest size. *Nature* **391**, 532-533 (1998).
9. Ogata, S., Li, J., Hirosaki, N., Shibutani, Y. & Yip, S. Ideal shear strain of metals and ceramics. *Physical Review B* **70**, 104104 (2004).
10. Shan, Z. W., Stach, E. A., Wieszorek, J. M. K., Knapp, J. A., Follstaedt, D. M. & Mao, S. X. Grain boundary-mediated plasticity in nanocrystalline nickel. *Science* **305**, 654-657 (2004).
11. Svelto, O. *Principles of Lasers* (Springer, 1998).
12. Cottrell, A. H. & Bilby, B. A. A Mechanism for the Growth of Deformation Twins in Crystals. *Philosophical Magazine* **42**, 573-581 (1951).
13. Christian, J. W. & Mahajan, S. Deformation Twinning. *Prog. Mater. Sci.* **39**, 1-157 (1995).
14. Niewczas, M. & Saada, G. Twinning nucleation in Cu-8 at.% Al single crystals. *Philosophical Magazine A* **82**, 167-191 (2002).
15. Dregia, S. A. & Hirth, J. P. A Rebound Mechanism for Lomer Dislocation Formation in Strained Layer Structures. *Journal of Applied Physics* **69**, 2169-2175 (1991).
16. Zhu, T., Li, J., Samanta, A., Kim, H. G. & Suresh, S. Interfacial plasticity governs strain rate sensitivity and ductility in nanostructured metals. *Proceedings of the National Academy of Sciences of the United States of America* **104**, 3031-3036 (2007).
17. Zhu, T., Li, J., Samanta, A., Leach, A. & Gall, K. Temperature and strain-rate dependence of surface dislocation nucleation. *Phys. Rev. Lett.* **100**, 025502 (2008).
18. Chen, M. W., Ma, E., Hemker, K. J., Sheng, H. W., Wang, Y. M. & Cheng, X. M. Deformation twinning in nanocrystalline aluminum. *Science* **300**, 1275-1277 (2003).
19. Suresh, S. & Li, J. MATERIALS SCIENCE Deformation of the ultra-strong. *Nature* **456**, 716-717 (2008).
20. Zhu, T., Li, J., Ogata, S. & Yip, S. Mechanics of Ultra-Strength Materials. *MRS Bulletin* **34**, 167-172 (2009).